

Existence of various structural zones in keratinous tissues revealed by X-ray microdiffraction

B. Busson,^a P. Engström^{b,c} and J. Doucet^{a*}

^aLURE, Centre Universitaire Paris-Sud, Bâtiment 209D, BP 34, F-91898 Orsay CEDEX, France, ^bKCK, Chalmers, S-41296 Göteborg, Sweden, and ^cESRF, BP 220, F-38043 Grenoble CEDEX, France. E-mail: doucet@lure.u-psud.fr

(Received 20 October 1998; accepted 24 March 1999)

Keratinous tissues play two major roles in the adaptation of vertebrates to their environment: a strong mechanical support and a chemical barrier. In order to determine whether these properties may originate from different zones in the tissues, microdiffraction experiments on the micrometre scale have been carried out on feather shaft, horse and human hair, and porcupine quill samples. The existence of several structural layers has been revealed in all the tissues, some corresponding to highly ordered α - or β -type keratin and the others to more or less amorphous keratin. The existence of lipid granules has also been evidenced, mainly in the outer layers. This study shows one of the possibilities which are now offered by third-generation synchrotron sources for the structural microanalysis of biological tissues.

Keywords: microdiffraction; biological tissues; keratinous tissues; α -keratin; feather keratin.

1. Introduction

Keratins form a class of sulfur-rich, mostly fibrous, proteins which are the main components of the tissues located at the 'surface' of higher vertebrates, *i.e.* the horny layer of epidermis and the appendages such as hair, nails, scales, quills, horns and feathers. They play essential roles in the adaptation of vertebrates to their natural environment, acting as a mechanical support but also as thermal and chemical barriers. Keratin-containing tissues were first studied for the economic importance of animal fibres in the textile industry, along with their medical- and cosmetic-related aspects such as hair growth and epidermis substitutes. A new impetus is now given by the polymer industry to understand the outstanding mechanical properties of keratin fibres in order to help in the development of synthetic fibres.

A first classification based on different modes of biosynthesis and corresponding to tactile sensation distinguishes 'soft' from 'hard' keratins (Giroud & Leblond, 1951). Soft keratins are found in the stratum corneum and calluses whereas hard keratins are the main component of hairs, nails, quills and claws. Soft keratins also contain less sulfur than hard keratins (Ward & Lundgren, 1954).

The second classification into four classes – α , β , feather and amorphous – is based on the X-ray scattering patterns (Fraser *et al.*, 1972). Hard mammalian keratinous tissues produce the typical α -pattern with a strong and narrow meridional reflection of spacing 5.15 Å and a broad equatorial one around 9.7 Å. Hard avian and reptilian tissues give the very rich feather pattern made up of many sharp

reflections (Astbury & Beighton, 1961). The β -pattern is produced by stretched mammalian keratin and looks similar to the feather pattern in some respects (Astbury & Street, 1931). The fourth class, called amorphous keratin, does not show any discrete reflections but only two diffuse haloes with maxima at spacings around 4.5 and 9.5 Å. It is observed, for instance, in the cuticle extracted from animal hair.

The quality of the X-ray diffraction patterns of keratins is not sufficient to lead to a full structure determination on an atomic scale. However, in the case of α - and β -types, a correspondence with secondary polypeptide structure has been established. In hard α -keratin, part of the chains are folded into α -helical coiled coils (Pauling *et al.*, 1951), and β -sheets are thought to characterize the β -class (Astbury & Woods, 1933). At higher scales, little is known except for hard α -keratin in which the 45 nm-long molecules are characterized by an alternation of coiled coil parts and non-helical segments. Keratin molecules are assembled both longitudinally and laterally, forming a very complex supercoil structure called microfibril (Parry & Steinert, 1995). The microfibrils are themselves embedded in a high sulfur protein matrix and packed by bundles into macrofibrils. This packing is characterized on X-ray diffraction patterns by three equatorial spots located at 88, 45 and 33 Å.

One of the major problems faced in X-ray diffraction pattern analysis of keratin-containing tissues is their heterogeneous character. The tissues are in fact composite materials including other constituents in addition to keratin, mainly proteins and lipids. Consequently, the

scattering contributions from the various constituents are superimposed in the patterns. The keratin itself may be present under several structural forms, for instance, α and amorphous. In this case, the scattering features of the α -part may be prominent in the pattern, even if the amorphous component is the predominant one in the tissue. Surprisingly there is a lack of microphotographic documentation on this subject. Several zones are visible on images of wool fibre sections (Rogers, 1959) but more attention has been paid to relate these zones to different biochemical contents than to structural microscopic characteristics (for a review, see Marshall *et al.*, 1991). The rather regular packing of microfibrils is apparent on electron microscopy images but these observations are very often focused on the best ordered zones in the tissues. In addition, the electron microscopy technique is not sensitive to molecular configuration in this type of material.

Up to now, scattering experiments have been performed with X-ray beams larger than 100 μm , consequently integrating large parts or the entire volume of a tissue. Since investigations with microbeams on the micrometric scale are now possible using third-generation synchrotron sources, we have taken advantage of this tool to reveal the existence of various structural zones in keratinous tissues and localize them. Such observations can greatly improve our knowledge on keratin structure and biosynthesis, and make it possible to follow structural modifications induced by chemical or mechanical treatments. This study exemplifies the possibilities which are now offered by microdiffraction for biological tissues analysis whilst revealing new features on keratin-containing tissues, the detailed analysis of the structure-properties relationship being out of its scope.

2. Materials and methods

2.1. Materials

Four keratinous materials have been analysed: three hard α -keratin samples – human hair, horse hair and porcupine quill – and peacock feather shaft for feather keratin. A small parallelepipedic piece of the 240 μm -thick shaft wall was cut out (approximate length along the feather axis 1 mm and width 1 mm) for scanning along the wall thickness. Two samples of horse hair from the tail (mean diameter 200 μm) were prepared: a 500 μm -long piece to be scanned with the X-ray beam parallel to the hair axis and a 40 μm -thick piece to be scanned with the beam perpendicular to the axis. The thickness of the latter was reduced from 200 to 40 μm by removing two pieces on opposite sides of the hair parallel to the axis, giving birth to a quasi-parallelepipedic sample as represented schematically in Fig. 4. This was achieved using an optical binocular microscope ($\times 100$ magnification) and cutting two opposite sides with a razor blade. Similarly, two samples of human hair (mean diameter 80 μm) were prepared with the same geometric characteristics (thickness ~ 40 μm after removing the two lateral pieces). The porcupine quill

sample (*Atherurus Africanus*) was prepared by cutting a 1 mm-long piece in a 1 mm-wide and 0.54 mm-thick quill, to be analysed with the beam either parallel or perpendicular to the quill axis. It is worth noting that the porcupine quill is not symmetric; the inner side in contact with the animal epidermis is planar whereas the outer side is groove-shaped.

2.2. Methods

Experiments were carried out at the ESRF on the microfocus beamline ID13 (Engström *et al.*, 1995). A high-intensity monochromatic beam from an undulator (wavelength 0.95 \AA) was focused and then size-limited down to a 2.3 μm -diameter circular section by a tapered glass capillary focusing optics (Bilderback *et al.*, 1994). A pinhole was added at the exit of the capillary to remove wide-angle scattering signals from glass. Taking into account the intrinsic glass capillary beam divergence (3 mrad), the beam diameter at the entrance side of the sample is estimated to be ~ 3 μm , and on the exit side of a 1 mm-long sample to be 6 μm .

Samples were mounted on a computer-controlled Physik Instrument *X/Y* stage coupled to a microscope which permitted them to be positioned in the beam with 0.1 μm spatial resolution. According to the samples and to the zones in a given sample, the step size between data points ranged from 2 to 10 μm . Prior to mounting on the *X/Y* stage, samples were mounted on a goniometer head and aligned using an optical two-circle reflection Huber goniometer at a 1° accuracy. This accuracy is limited by the deviations of biological tissues shapes from perfect planar or linear figures. A key point for the reliability in the experiment was to make sure that the beam was not travelling through different structural zones along the sample. A misalignment of 1° corresponds to a deviation of

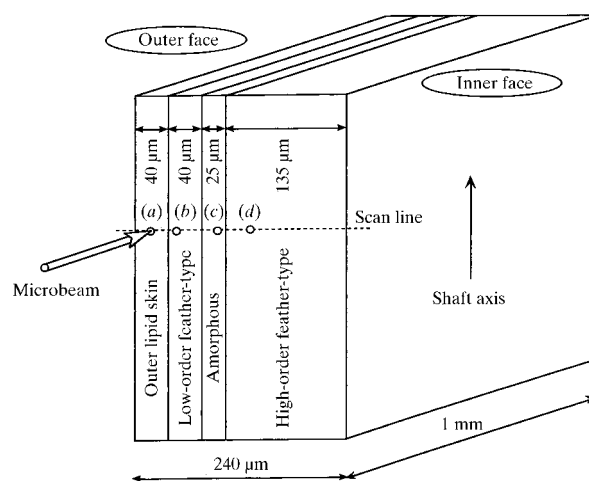


Figure 1

Schematic representation of a feather shaft wall section showing the four structural zones, the scan line corresponding to Fig. 2 (dotted line) and the positions (a), (b), (c) and (d) corresponding to the patterns of Fig. 3.

18 μm for a 1 mm-long path. We have checked that this value was smaller than the thickness of the structural zones which were detected on the feather shaft and the porcupine

quill. Otherwise, thinner samples should have been prepared. The situation was different for hair because of the cylindrical geometry which in perpendicular geometry

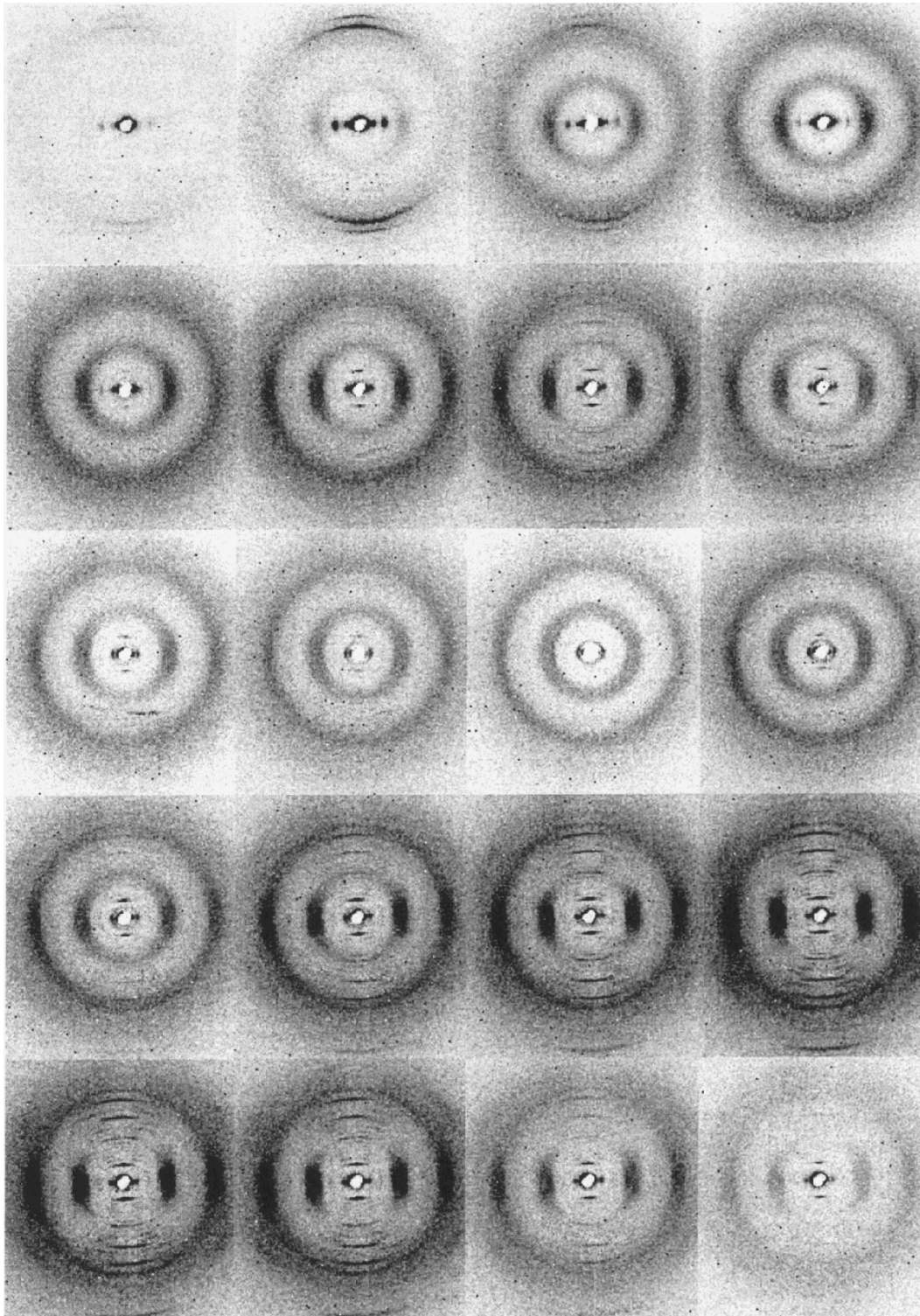


Figure 2

Series of scattering patterns of a feather shaft wall section, recorded with the beam perpendicular to the shaft axis (vertical), along the scan line represented in Fig. 1. From left to right and then top to bottom, the positions starting from the outer face to the inner face of the shaft correspond to the following depths in micrometres: 5, 25, 28, 30, 35, 60, 70, 78, 82, 90, 100, 110, 112, 114, 118, 145, 175, 195, 215 and 235. The intensity grey scale is linear.

leads to an overlap of the scattering features coming from different zones. We have tried to minimize this effect by removing part of the hair as explained in §2.1. However, the accuracy of the alignment was not sufficient to detect the signal from the very thin layer cuticle alone.

Wide-angle scattering patterns were recorded on a Photonic Science CCD camera located at 280 mm from the sample. The exposure time was 10 s but, in order to increase the signal-to-noise ratio without degrading the sample by a too high thermal load, two images were

recorded at each position and then added (with the beam shutter closed for a few seconds between the two exposures).

3. Results

The results presented in this part are deduced from a combination of the analyses performed in the various geometries described in §2.1.

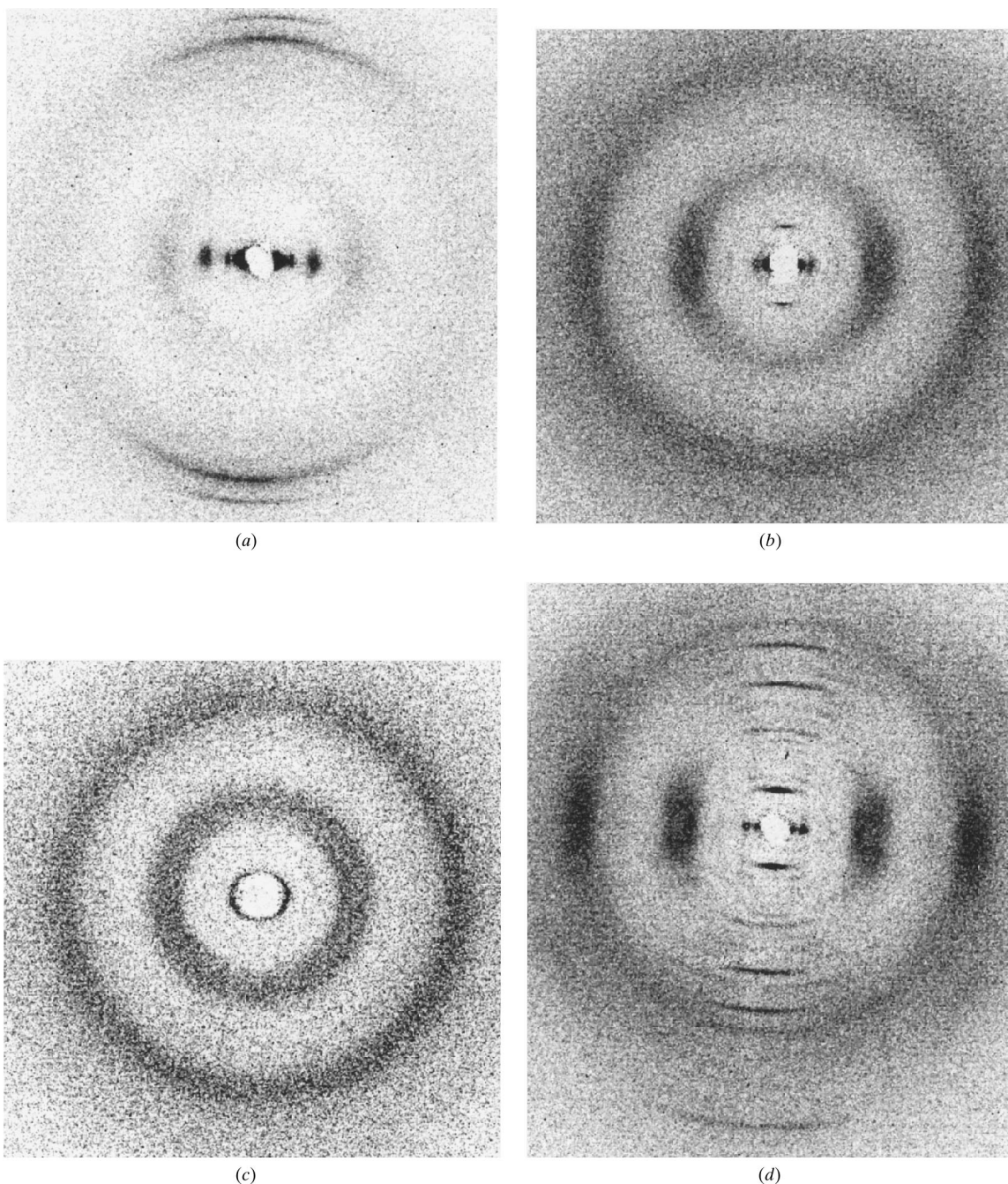


Figure 3

Typical feather shaft microdiffraction patterns in the four structural zones; the shaft axis is vertical. The distances to the outer face are as follows. (a) 20 μm : outer lipid layers zone; a faint signal from keratin is also visible. (b) 50 μm : moderately ordered feather-type keratin zone. (c) 100 μm : isotropic amorphous keratin zone. (d) 150 μm : highly ordered feather-type keratin zone.

3.1. Feather shaft

The scan of the feather shaft (Fig. 1) reveals four structural zones with very different scattering patterns (Figs. 2 and 3). The pattern observed in the outer 40 μm -thick zone (Fig. 3a) is typical of a lipid layer stack lying parallel to the surface of the shaft wall since the reflections from the layers are aligned along the normal to the wall. The two sharp high-angle arcs reveal a crystalline ordering of the lipid chains within the layers. This pattern is similar to that given by the intercellular lipids of stratum corneum (Garson *et al.*, 1991). The pattern of the next zone, which is also 40 μm thick, corresponds to a moderately ordered feather-type keratin (Fig. 3b). Keratin molecules are lying preferentially in the plane of the wall, parallel to the shaft axis, as attested by the reinforcing of the rings at 9.6 and 4.6 \AA along the equator. The third zone (25 μm -thick) surprisingly displays a pattern of amorphous keratin without any preferential orientation of the molecules (Fig. 3c). The highly crystallized feather keratin pattern, with many sharp reflections, is observed in the fourth zone which starts at $\sim 105 \mu\text{m}$ from the outer surface and persists 135 μm down to the inner one (Fig. 3d). The molecules are oriented, as in the second zone, parallel to the shaft axis. It must be noted in Fig. 2 that the transitions between the various zones are progressive, with possible coexistence of two types of structure.

From these observations it can be concluded that the classical feather-type pattern is only produced by about half of the sample. In addition to the lipid-rich skin, other zones

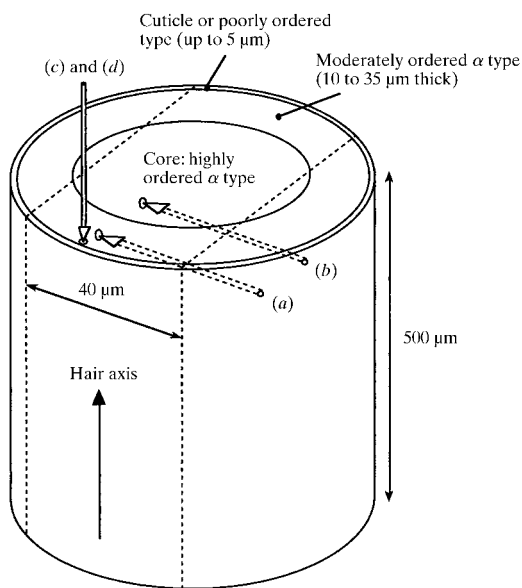


Figure 4
Schematic representation of a hair section showing the three structural zones. The dotted lines show the almost parallelepipedic shape obtained after cutting the sample for the perpendicular geometry analyses. The cuticle is represented though it has not been convincingly detected by microdiffraction. The diameter of the two outer zones is almost independent of hair diameter, whereas the core diameter is not. Positions (a), (b), (c) and (d) corresponding to the patterns of Fig. 5 are also indicated.

characterized by much poorly ordered keratin are observed, but their scattering features are less intense than the strong reflections from the ordered feather-type keratin. Nevertheless, we have checked that the features of the four zones appear on the scattering pattern of the entire sample using a large beam size (300 μm). We have proved here by microdiffraction analysis that they proceed from four different structural separated layers and not from zones distributed homogeneously within the feather wall.

3.2. Horse and human hair

These two samples are very similar: three structural layers have been detected, scanning from the outside towards the centre of the hair (Fig. 4). Below 2–5 μm , low-intensity diffuse rings at ~ 9.6 and 4.5 \AA indicate a poorly ordered organization. Because of the very small thickness (2 μm) of the cuticle (outermost layer of the hair), it is difficult to conclude whether they are produced by the cuticle itself or by amorphous keratin located in the cortex. Then, in the second zone, ~ 15 –35 μm thick for horse hair and 10–15 μm for human hair, the typical scattering features of hard α -keratin (9.7 \AA equatorial and 5.15 \AA meridional reflections) progressively appear, revealing a gradual ordering of the molecular organization, the molecules being parallel to the hair axis (Fig. 5a). The third zone corresponds to the core of the hair for which the pattern is typical of highly ordered hard α -keratin (Fig. 5b).

As for feather shaft, only about half the tissue is strongly ordered and progressive organization is observed. It is interesting to note that the signals from the coiled coil structure (9.7 \AA equatorial and 5.15 \AA meridional reflections) appear simultaneously with the diffraction spot from the microfibrils on the equator (only the third order at 33 \AA can be detected on our wide-angle patterns). The structuring of keratin organization seems to be concerted from the coiled coil scale to the microfibril one.

Scattering features from lipids are also present on hair patterns. They correspond to a lamellar periodicity of about 45 \AA , and rings at spacings 4.1 and 3.7 \AA – characteristic of the order within the layers – are also sometimes visible. From the angular width of the 45 \AA ring [Scherrer equation (Guinier, 1963)], it can be deduced that the lipids are stacked within 500–1000 \AA -thick granules. Granules are spread in all the cortex without any specific orientation *versus* hair axis. In the first 10 μm under the hair surface, the lipid signals are very intense, even more than keratin signals, which reveals the existence of a highly concentrated zone of lipids in and just under the cuticle (Fig. 5c). The lipid signals, which coexist with poorly ordered keratin, progressively decrease while the keratin signals increase. A possible interpretation is to assume a link between the existence of poorly ordered keratin and lipids. Let us finally mention an interesting difference between human and horse hair: the lipid layers in the outer zone lie parallel to the surface for horse hair (diffraction limited to arcs as seen in Fig. 5d), whereas no specific orientation is noted for human hair (full diffraction rings as seen in Fig. 5c). For

horse hair, this supports, but does not prove, the hypothesis of a continuous lipid layer organization parallel to the surface and may be of a stronger chemical barrier than for human hair.

3.3. Porcupine quill

Porcupine quills are known to display the best quality diffraction patterns for hard α -keratin (MacArthur, 1943), which indicates a highly crystallized structure. As for feather shaft and hair, we have observed that only part of the material is highly organized. The porcupine quill is in fact made up of a stack of layers lying parallel to the outer (in contact with environment) and inner (in contact with

the animal) faces, among which only two correspond to a highly organized structure. As the frontiers between the various layers are not abrupt but progressive, the description of the structure may be debatable all the more since the thickness of the layers is not only simply dependent on the thickness of the quill but may also vary from one point to a neighbouring one on the same sample. We estimate that a 'first approximation' description in terms of two layers located symmetrically with respect to a middle one (five layers overall, see Fig. 6) is reasonable and compatible with our microdiffraction data.

Scanning from the outer to the inner layers (Fig. 7), the first layer corresponds to hard α -keratin structure, rather

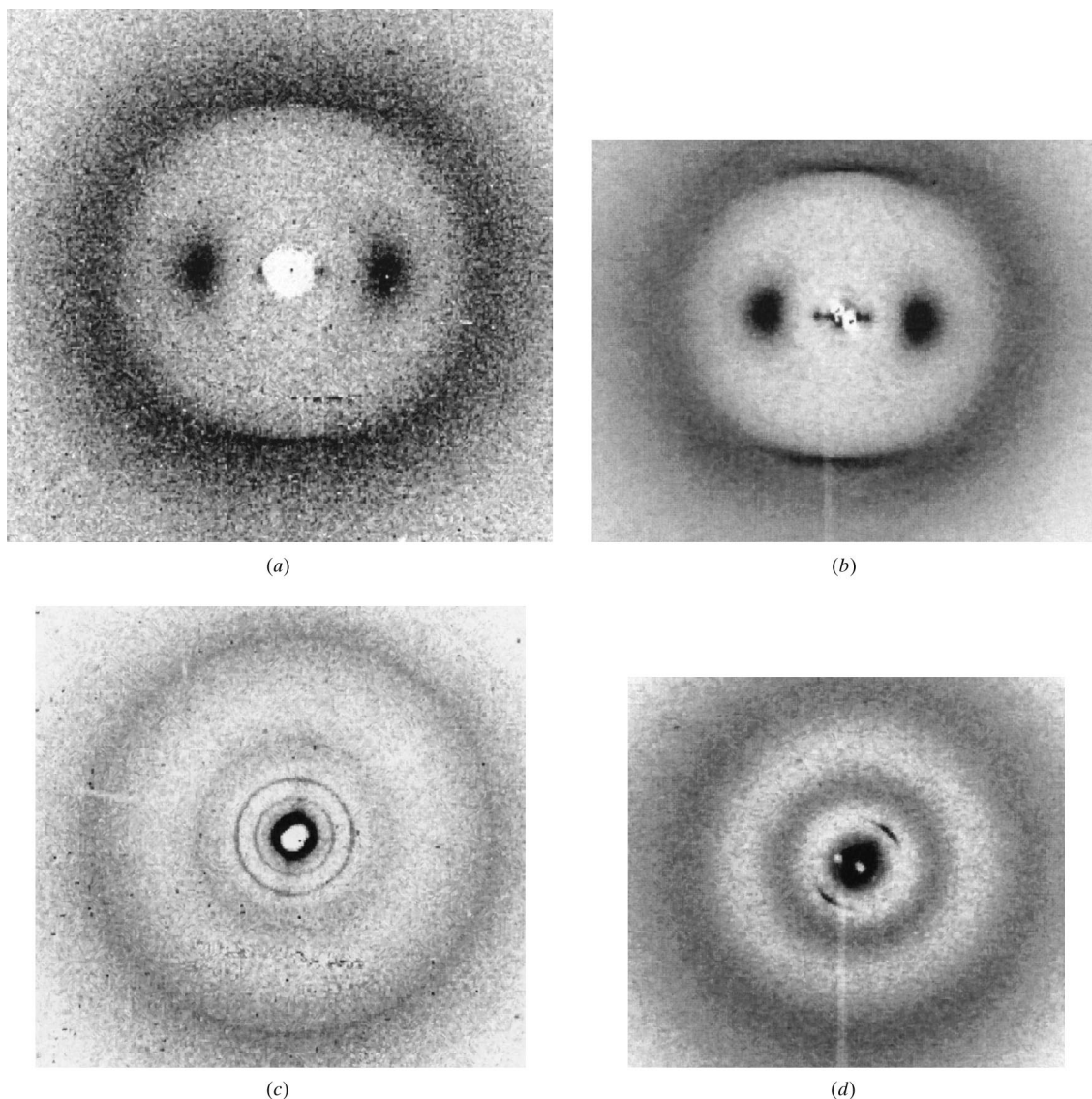


Figure 5

Hair microdiffraction patterns in linear intensity grey scale. (a) Pattern of the outer zone of horse hair in perpendicular geometry, 7 μm under the surface (hair axis is vertical). The keratin is moderately ordered α -type. (b) Pattern of the horse-hair core in perpendicular geometry ($\sim 50 \mu\text{m}$ below the surface). Strong typical features of hard α -keratin are visible (hair axis is vertical). (c) Diffraction signals from lipid granules in the outer zone of human hair in parallel geometry (3 μm under the surface). The diffraction rings indicate a random orientation of the stacks. (d) Diffraction signals from lipid granules in the outer zone of horse hair in parallel geometry (3 μm under the surface). The diffraction arcs indicate a preferential orientation parallel to the surface.

poorly ordered close to the surface but which progressively becomes more ordered after 20–70 μm (even highly ordered for the internal side) and persists for a few more tens of micrometres as attested by the strong characteristic diffraction features (Fig. 8a). The molecules in this layer are oriented parallel to the quill axis. An important difference between the outer and inner sides must be pointed out: scattering signals from crystallized lipids are not observed in the inner side layer whereas strong reflections in the outer one, down to $\sim 70 \mu\text{m}$, correspond to stacks lying parallel to the surface (Fig. 8b). We favour the idea that these lipids play a protection role from external aggressions, which is not necessary for the inner face of the quill. Let us note in Fig. 8(b) the presence of strong and sharp equatorial arcs at 7.1 and 3.5 \AA . Their origin is not known, but they appear to be related to keratin because they have also been observed in stratum corneum X-ray scattering patterns (Garson *et al.*, 1991).

In the second layer, hard α -keratin signals progressively disappear, which is indicative of a transformation towards a less-ordered keratin organization (Fig. 8c). It is interesting to note that the 5.15 and 30 \AA reflections, which are characteristic of the coiled coil and microfibril structure, respectively, disappear simultaneously, which means that the coiled coil and microfibril levels of organization are probably mutually stabilized. This transformation towards amorphous keratin is accompanied by a disorientation effect, clearly visible on the equatorial 9.7 \AA spots which are transformed into a ring, but still reinforced along the normal to the surface. This means that the fluctuations of the molecular orientations around the quill axis are large.

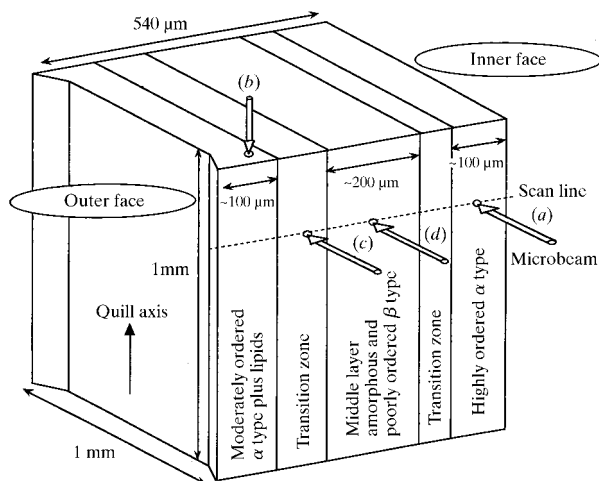


Figure 6 Schematic representation of a porcupine quill section showing the five structural zones located more or less symmetrically with respect to the middle layer. The external surface corresponds to the outer and the inner surface to the side in contact with the animal. The layer thicknesses depend on the overall quill thickness and on the position along the quill. The scan line corresponding to Fig. 7 (dotted line) and the positions (a), (b), (c) and (d) selected in Fig. 8 are also indicated.

The typically 200 μm -thick middle layer corresponds to amorphous keratin with no sharp scattering signals but only diffuse rings at ~ 4.6 and 9.6 \AA . However, on some patterns the 9.6 \AA ring is strongly anisotropic and a rather sharp ring at 4.65 \AA is observed (Fig. 8d). Such features are comparable with poorly ordered β -keratin (Fraser *et al.*, 1972). The middle layer, which seems to be made of a mixture of amorphous and poorly ordered β microdomains, may be representative of a transition state between α - and β -type keratins (Feughelman & Mitchell, 1968).

4. Discussion and conclusion

We have shown here that the microdiffraction technique can be successfully used to analyse keratinous samples. This technique is quite sensitive for revealing the existence of zones with various keratin organizations on a scale of a few micrometres. This is due to the fact that, like many biological tissues, *e.g.* skin, keratinous tissues have a multilayer structure parallel to their surface with layer thicknesses of a few tens of micrometres. The layered structure and its long-range homogeneity parallel to the surface could therefore be reasonably expected for keratinous samples. On the contrary, the sequence of the layers could not be easily predicted, nor the fact that the sequences were similar. Common features have been observed for the four studied samples, *i.e.* feather shaft, human and horse hair, and porcupine quill, as follows.

(i) The different structural zones form layers lying parallel to the surface of the sample, which rules out the possibility of various structural domains mixed in a homogeneous sample on the macroscopic scale; keratinous samples can be considered as layered composite materials. The transitions between the contiguous zones are progressive, no discontinuity has been observed.

(ii) Lipid layer stacks have been detected in the first tens of micrometres below the surface, except for the inner side of the porcupine quill; they could play a barrier role towards the environment. Let us also note the presence of lipid granules within ordered α -keratin zones located in the cortex of human and horse hair.

(iii) Highly ordered keratin zones coexist with poorly ordered or even amorphous zones; the amount of ordered material giving rise to the well defined diffraction features represents between 50 and 75% of the total volume. Hard α -keratinous tissues also contain zones where keratin organization seems to be the same as in soft α -keratinous tissues. It is worth mentioning that the analyses carried out on extracted keratin molecules integrate molecules from different zones, thus limiting the significance of such analyses for structural aspects.

(iv) Finally, it seems that the structure on the molecular scale (α -helical coiled coils or β -sheets) and supramolecular scale (microfibrils) are intimately linked. In hard α -keratin, for instance, the coiled coil and microfibril structures are

always observed together and even appear or disappear simultaneously in the transition zones.

It is also interesting to note the similarity between the sequences of layers in the feather shaft and the porcupine quill. The external layer (*i.e.* in contact with the outside

world) is moderately ordered and contains large amounts of lipids, the internal layer (*i.e.* not in contact with the outside world) is highly ordered and does not contain any lipids. Between these two layers one finds poorly ordered or amorphous zones. This description can also be extended

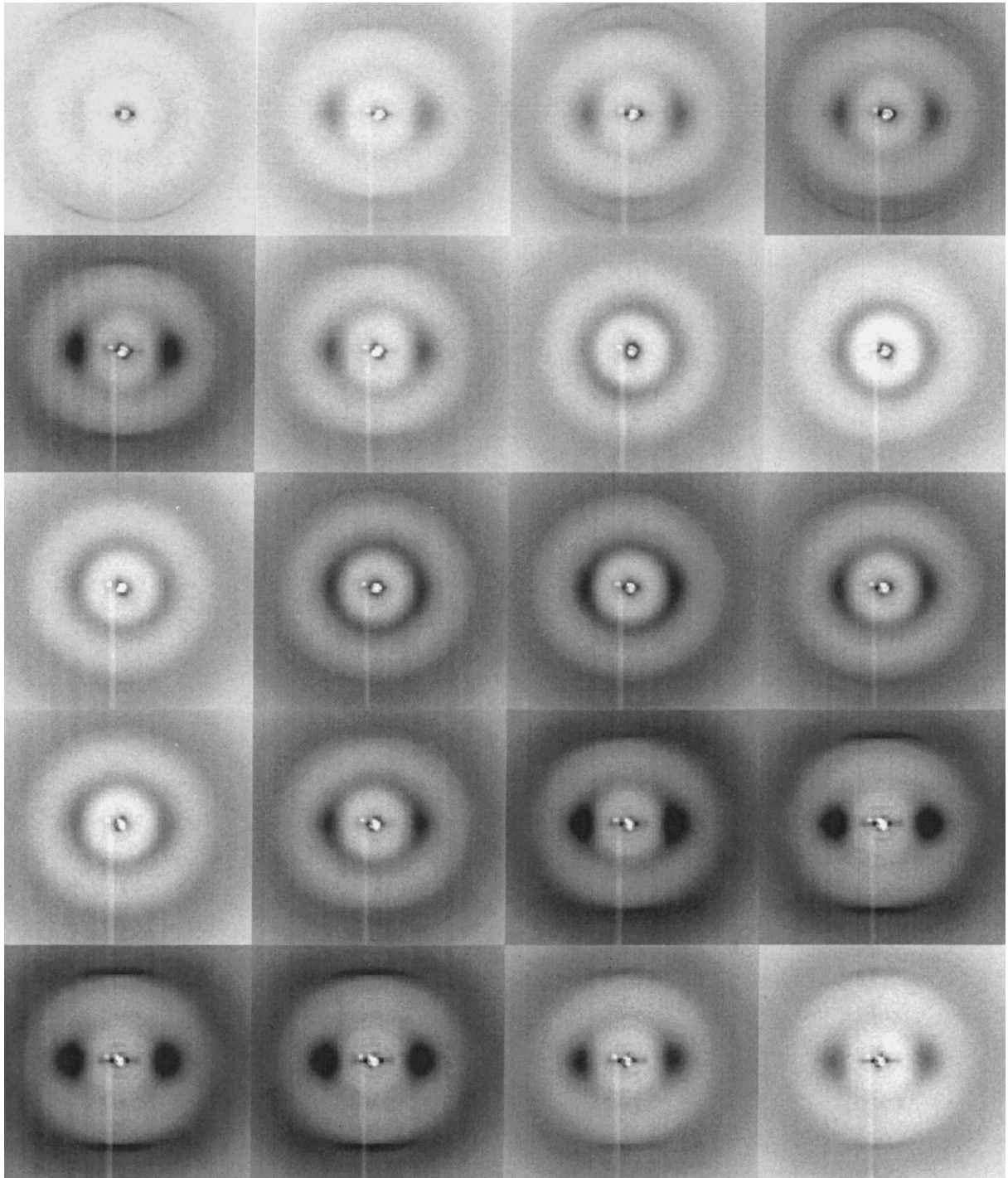


Figure 7

Series of scattering patterns of a porcupine quill section, recorded with the beam perpendicular to the quill axis (vertical), along the scan line represented in Fig. 6. From left to right and then top to bottom, the positions starting from the outer face of the quill to the inner face correspond to the following depths in micrometres: 5, 15, 30, 60, 90, 120, 150, 185, 220, 225, 285, 320, 350, 380, 410, 440, 470, 500, 530 and 535. The intensity grey scale is logarithmic.

to hair though the middle zone is missing, probably because of the smaller thickness of hair. From the layer sequence similarity it is tempting to surmise that the internal highly structured zones ensure the mechanical support of the tissue whilst the moderately ordered external ones with a lipid component would act as chemical and physical barriers; the middle layers would just fill the space between the outer layers, without any major role. However, the reason for the existence of various structural zones with almost the same biochemical content is, of course, beyond the scope of this paper and thorough analyses and comparisons between histological, biochemical and structural data would be necessary to establish correlations between functions and structures in keratinous tissues.

The microdiffraction technique offers new possibilities for the structural analysis of biological tissues, in particular

sequence, thickness and nature of the various structural zones. This technique can provide complementary information compared with electron microscopy, which has a better spatial resolution but cannot easily provide information on the molecular and supramolecular scales. In addition, no sample preparation is required and sample behaviour can be followed while varying parameters such as temperature, humidity or chemical environment. Microdiffraction should soon become an efficient tool for analysing human, animal and plant tissues.

We thank Dr M. Tranier from the Muséum d'Histoire Naturelle (Paris) for kindly providing us with the porcupine quill samples. We would also like to thank the ESRF staff, especially the ID13 beamline team, Dr C. Riekkel, Dr F.

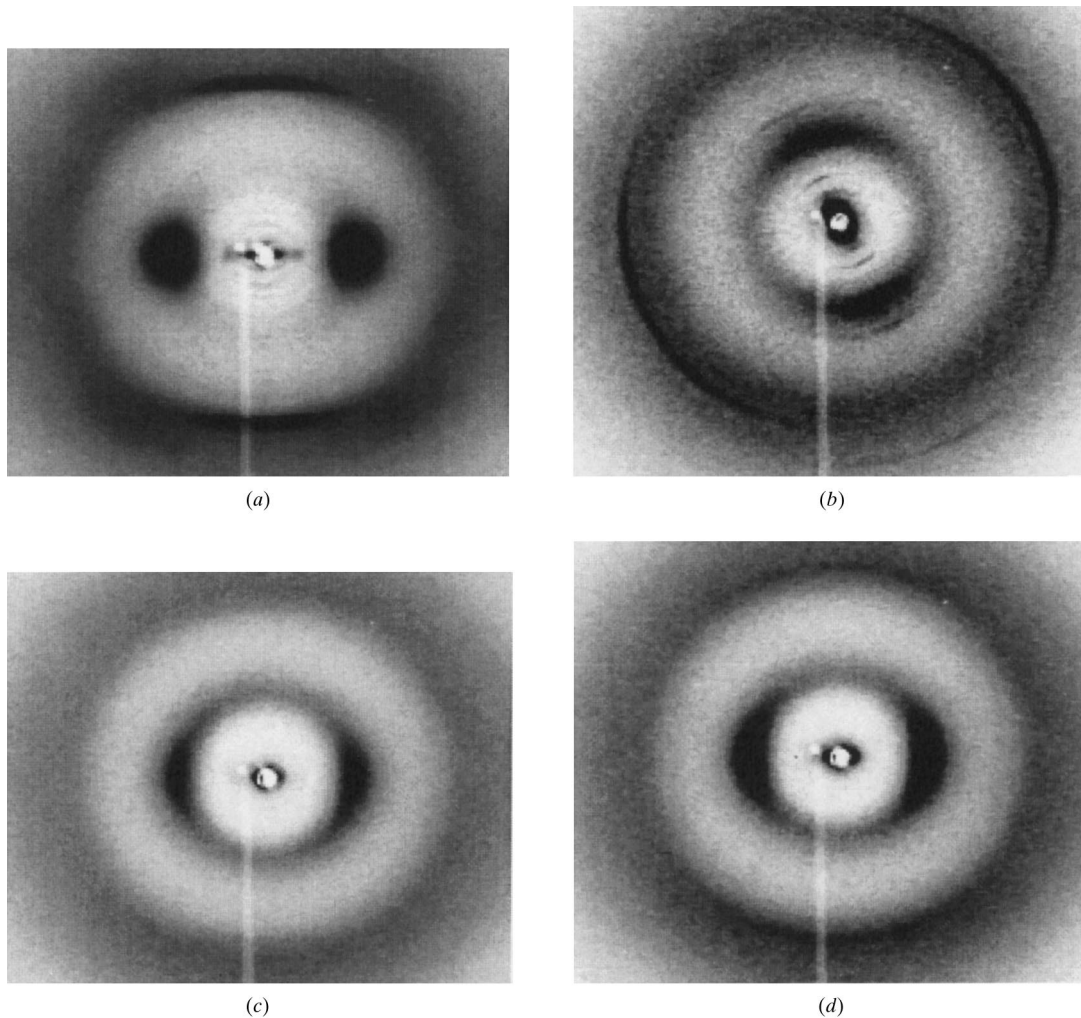


Figure 8

Typical porcupine quill microdiffraction patterns. (a) Typical pattern of a highly ordered α -type zone in perpendicular geometry. (b) Pattern obtained in the outer moderately ordered α -type zone in parallel geometry. Strong and sharp diffraction arcs due to lipid stacks are clearly visible. Unexplained arcs at 7.1 and 3.5 Å can also be seen. The anisotropy of the 9.7 Å ring intensity indicates that fibres are not parallel to the incident beam, *i.e.* to the quill axis. (c) Pattern in the transition zone in perpendicular geometry; the 5.15 and 30 Å features have disappeared. (d) Pattern in the middle zone in perpendicular geometry. A rather sharp arc at 4.65 Å, typical of poorly ordered β -type, is visible.

Heidelbach and Dr A. Bram, for their help during the experiments and Dr A. P. Hammersley for the data analysis software *Fit2D*.

References

- Astbury, W. T. & Beighton, E. (1961). *Nature (London)*, **191**, 171–173.
- Astbury, W. T. & Street, A. (1931). *Philos. Trans. R. Soc. London*, **A230**, 75–101.
- Astbury, W. T. & Woods, H. J. (1933). *Philos. Trans. R. Soc. London*, **A232**, 333.
- Bilderback, D. H., Thiel, D. J., Pahl, R. & Brister, K. E. (1994). *J. Synchrotron Rad.* **1**, 37–42.
- Engström, P., Fiedler, S. & Riekkel, C. (1995). *Rev. Sci. Instrum.* **66**, 1348–1350.
- Feughelman, M. & Mitchell, T. W. (1968). *Biopolymers*, **6**, 1515–1518.
- Fraser, R. D. B., MacRae, T. P. & Rogers, G. E. (1972). *Keratins*. Springfield, IL: Charles Thomas Publishers.
- Garson, J. C., Doucet, J., Lévêque, J. L. & Tsoucaris, G. (1991). *J. Invest. Dermatol.* **96**, 40–49.
- Giroud, A. & Leblond, C. P. (1951). *Ann. NY Acad. Sci.* **53**, 613–626.
- Guinier, A. (1963). *X-ray Diffraction in Crystals, Imperfect Crystals and Amorphous bodies*. San Francisco: W. H. Freeman.
- MacArthur, I. (1943). *Nature (London)*, **152**, 38–41.
- Marshall, R. C., Orwin, D. F. G. & Gillespie, J. M. (1991). *Electron Microsc. Rev.* **4**, 47–83.
- Parry, D. A. D. & Steinert, P. M. (1995). *Intermediate Filament Structure*. Berlin: Springer-Verlag.
- Pauling, L., Corey, R. B. & Branson, H. R. (1951). *Proc. Natl Acad. Sci.* **37**, 205–211.
- Rogers, G. E. (1959). *Ann. NY Acad. Sci.* **83**, 378–399.
- Ward, W. H. & Lundgren, H. P. (1954). *Advances in Protein Chemistry*, edited by M. L. Anson, K. Bailey & J. T. Edsall, Vol. 9, pp. 243–297. New York: Academic Press.